

Modelling of magnetic field structure of the Ergodic Divertor of Tore Supra and comparison to the Dynamic Ergodic Divertor of TEXTOR

S.S. Abdullaev¹, T. Van Rompuy², K.H. Finken¹, M. Lehnen¹, M. Jakubowski¹

¹Institut für Energieforschung–4, Forschungszentrum Jülich GmbH, EURATOM Association, D-52425 Jülich Germany,

²Department of Applied Physics, Ghent University
Rozier 44, B-9000 Gent, Belgium

May 9, 2008

Abstract

An analytical model previously developed to study the structure of the magnetic field for the TEXTOR-DED [S.S. Abdullaev et al. *Phys. Plasmas*, **6**, 153 (1999)] is applied to the similar study of the Ergodic Divertor of Tore Supra tokamak [Ph. Ghendrih, *Plasma Phys. Control. Fusion*, **38**, 1653 (1996)]. The coil configuration of ED Tore Supra consists of six modules equidistantly located along the toroidal direction on the low-field-side of the torus with given toroidal and poloidal extensions. The Hamiltonian formulation of field line equations in straight-field-line coordinates (Boozer coordinates) and the computationally efficient mapping method for integration of the Hamiltonian field line equations are used to study the magnetic field structure in the ED. Asymptotical formulas for the perturbation magnetic field created by the ED coils are obtained and the spectrum of magnetic perturbations is analyzed and compared with the one of the TEXTOR-DED. The structure of ergodic and laminar zones are studied by plotting Poincaré sections, so-called laminar plots (contour plots of wall to wall connection lengths) and magnetic footprints. The radial profiles of field line diffusion coefficients are calculated for different perturbation currents and it is found that for the Tore Supra case in the ergodic zone the numerical field line diffusion coefficients perfectly follow the quasilinear formula for smaller perturbation currents although the situation is different for the maximum perturbation current.

1 Introduction

The problem of plasma–wall interaction is one of the key issues in nuclear fusion research. To control the plasma edge, the concept of an ergodic divertor has been proposed in Refs. [1–3]). The idea of the ergodic divertor is based on the creation of a stochastic zone of magnetic field lines open to the plasma wall which would guide the ionized particles and energy to special divertor plates, and prevent the penetration of wall-released impurities into the plasma core. The stochastic field lines at the plasma edge should be formed by externally created resonant magnetic perturbations using external coils.

The ergodic divertor (ED) (ergodic limiter) has been later implemented in several large size and small size tokamaks. Particularly, an ergodic limiter has been installed in TEXT (Refs. [4–9]), in Tore Supra (Refs. [10–17]) and in a number of small-size tokamaks (in JFT-2M ([18, 19]), CSTN-II ([20, 21]), HYBTOK-II ([22]), TBR-1 [23], TCABR ([24]), and other small fusion devices ([25, 26]).

The ergodic divertor implemented in the TEXTOR tokamak, the Dynamic Ergodic Divertor (DED) [27–29], has dynamical features in addition to the conventional ones. It permits the operation with a rotating magnetic perturbation field, which allows not only to broaden the heating footprints to avoid hot spots on the divertor plates but also to actively influence the plasma rotation and MHD activities [30, 31]. At the same time the DED perturbation field has an influence on runaway electron dynamics [32, 33], spontaneous density built-up [34], and reduction of turbulence transport [35]. Particularly, the DED perturbation field has been used to control edge localized modes (ELM) in limiter H-mode plasmas [33], similarly to the recent experiments in the DIII-D tokamak to suppress ELM by the external resonant magnetic perturbations [37–39].

The energy and particle transport in the ergodic zone depends significantly on the structure of the perturbation magnetic field at the plasma edge. Numerous recent experiments on the TEXTOR-DED have demonstrated that the transport along the field lines in the presence of the resonant magnetic perturbations becomes predominant and prevails over the cross field neoclassical and anomalous diffusion [40]. The field lines even determine a fine structure of heat deposition patterns [41–43], which is mainly due to the reduction of the large scale turbulence level at the plasma edge during DED operation [35, 36]. Therefore the study of the magnetic field structure is an important first step in understanding the transport properties of the plasma edge modified by the resonant magnetic perturbations.

Traditional methods to study the perturbation field structure and its statistical properties in ergodic divertors have been mainly based on numerical codes [44–47]. One of the approaches to study the formation of the ergodic zone of field lines is based on the direct field line tracing in a toroidal system (see, e.g., [46]). More in particular, to study the perturbation magnetic field structure in the ED of Tore Supra the MASTOC code has been developed. In its early version [44], the field lines equations are formulated in a Hamiltonian form using the intrinsic coordinates. The Fourier coefficients of the perturbation Hamiltonian are found

by direct integration along the unperturbed field lines using the Biot and Savart formula and the field line equations are integrated by the Runge–Kutta integration scheme.

A new approach to study this problem with an application to the TEXTOR-DED has been developed in Refs. [48–51]. This approach consists of two steps. The first step is to formulate the equations of magnetic field lines in Hamiltonian form using the magnetic flux coordinates. For this purpose the analytical models for the external coil configurations and the equilibrium magnetic field of the plasma are used [48,49,51]. In the second step the Hamiltonian equations are integrated using the computationally effective symplectic mapping methods developed in Refs. [52–54]).

In this work we shall apply these analytical and mapping methods to study the perturbation magnetic field structure in the ED of Tore Supra.

The paper consists of three sections. In Sect. 2 we consider a model for the ED perturbation coils, analytically calculate the perturbation magnetic field and study its poloidal and toroidal spectra, as well as its radial dependence. There we also study the poloidal spectrum of the perturbation magnetic field in magnetic flux coordinates, its relation with the corresponding spectrum in geometrical coordinates, and compare with the spectrum of the TEXTOR-DED perturbation field. The structure of the ergodic zone created by the perturbation field and the statistical properties of chaotic field lines are studied in Sect. 3 using different methods, ranging from the qualitative Chirikov criterium to the quantitative methods as Poincaré sections, laminar plots and magnetic footprints. In addition, we calculate the radial profiles of the field line diffusion coefficients. The summary of obtained results is presented in the conclusive section.

2 ED coil configuration, perturbation magnetic field and perturbation spectra

Tore Supra is a large size tokamak with superconducting toroidal coils. Its major radius is $R_0 = 2.38$ m and the minor radius $a = 0.8$ m. The ED coil configuration consists of six identical modules located on the low field side of the torus and equidistantly spaced along the toroidal angle φ [11,44]. Each module has a poloidal extension $\Delta\theta \approx 2\pi/3$ and a toroidal extension $\Delta\varphi \approx 2\pi/14$. The modules are located at the minor radius $r_c = 85$ cm.

We model the module with a coil winding shown in Fig. 1 where arrows indicate the current direction. The current flows from the feeder located at the beginning of the first section $j = 1$ of the inner side of the winding shown in Fig. 1a and returns through the outer side of the winding shown in Fig. 1b. The minor radii of the inner and outer sides are $r_{c1} = 84$ cm $r_{c2} = 86$ cm, respectively ¹. Below we calculate the magnetic field, created by the current flowing in this coil system

¹Furthermore, we use the quasitoroidal coordinate system (r, θ, φ) , which will be referred as geometrical coordinates.

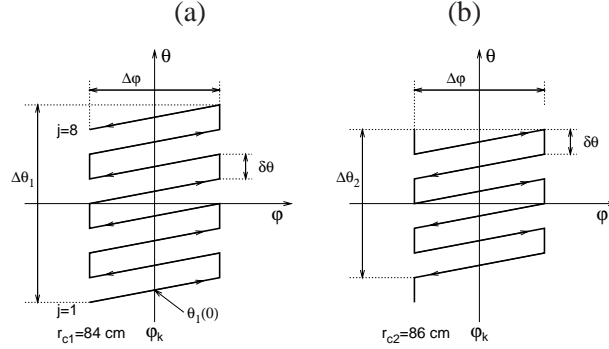


Figure 1: Model scheme of one module of the ED coils: (a) the inner winding at $r_{c1} = 84$ cm; (b) the outer winding at $r_{c2} = 86$ cm.

by considering, in a first time, the case of inner and outer parts of the winding separately, and by summing those parts afterwards.

Suppose that the modules are centered near the toroidal angles $\varphi_k = (k - 1)\Delta\varphi$, $\Delta\varphi = 2\pi/6$. The poloidal angle as a function of the toroidal angle of a point located in the j -th section in the k -th module ($k = 1, 2, \dots, 6$) is given by

$$\theta_j^{(k)}(\varphi) = \theta_1^{(k)}(\varphi) + (j - 1)\delta\theta, \quad j = 1, 2, \dots, N, \quad (1)$$

where $N = 8$ for the inner winding and $N = 6$ for the outer winding, and $\delta\theta$ is the poloidal spacing shown in Fig. 1. The coordinates of the first coils on each module are described by

$$\begin{aligned} \theta_1^{(k)}(\varphi) &= \theta_1(0) + \alpha(\varphi - \varphi_k), \\ \text{for } \varphi_k - \frac{\Delta\varphi}{2} < \varphi < \varphi_k + \frac{\Delta\varphi}{2}, \end{aligned} \quad (2)$$

where α is the slope of a coil creating a helical magnetic perturbation.

The poloidal extension, $\Delta\theta$, of a module shown in Fig. 1 can be expressed as a function of the poloidal position of the first coils, $\theta_1(0)$, at the toroidal section $\varphi = \varphi_k$:

$$\Delta\theta = 2|\theta_1(0)| + \alpha\Delta\varphi. \quad (3)$$

One should note that this model of coils is not fully equivalent to the Tore Supra coils. In the latter case the distance between sections of coils in each module are not equidistant along the poloidal angle θ . It slightly decreases with the distance from the equatorial plane $\theta = 0$ [55].

2.1 Current density

We describe the current, I_j , which flows in a coil section by

$$I_j^{(i)} = I_d \cos(\pi j) = (-1)^{j+1}, \quad j = 1, 2, \dots, N, \quad (4)$$

where I_d is the current flowing in the coil, $i = 1$ for the inner part of the winding and $i = 2$ for its outer part.

Below we shall consider only the long helical section coils since they create the magnetic field perturbations that are resonant with the magnetic field lines of the plasma. The vertical short sections of coils do not contribute to the resonant field, therefore they will not be taken into account.

One can introduce the current density vector $\vec{j}(r, \theta, \varphi)$ of the coil system as

$$\vec{j}_i(r, \theta, \varphi) = \vec{e}^{(i)} \frac{\delta(r - r_{ci})}{r_{ci}} \sum_{k=1}^6 g_\varphi^{(k)}(\varphi) \sum_{j=1}^N I_j^{(i)} \delta\left(\theta - \theta_j^{(k)}(\varphi)\right), \quad (5)$$

where $\vec{e}^{(i)} = (\vec{e}_r, \vec{e}_\theta, \vec{e}_\varphi) = (0, \sin \alpha_{0i}, \cos \alpha_{0i})$ is a unit vector along the helical section of the coils, $\alpha_{0i} = \alpha r_{ci}/R_c$, $R_c = R_0 + r_{ci}$, ($i = 1, 2$). Here $g_\varphi^{(k)}(\varphi)$ is a step function of the toroidal angle φ which takes a non-zero value in the areas covered by coils, i.e.,

$$g_\varphi^{(k)}(\varphi) = \begin{cases} 1, & \text{for } \varphi_k - \frac{\Delta\varphi}{2} < \varphi < \varphi_k + \frac{\Delta\varphi}{2}, \\ 0, & \text{elsewhere,} \end{cases} \quad (6)$$

Introducing the step function $g_i(\theta)$ solely depending on the poloidal angle

$$g_i(\theta) = \begin{cases} 1, & \text{for } -\frac{\Delta\theta_i}{2} < \theta < \frac{\Delta\theta_i}{2}, \\ 0, & \text{elsewhere,} \end{cases} \quad (7)$$

the current density (5) can after some transformations be reduced to

$$\begin{aligned} \vec{j}_i(r, \theta, \varphi) &= \vec{e}^{(i)} \delta(r - r_{ci}) J_0^{(i)} g_i(\theta) \sum_{k=1}^6 g_\varphi^{(k)}(\varphi) \\ &\times \sum_{s=-\infty}^{\infty} \cos\{m_0(2s-1)[(\theta - \theta_0) - \alpha(\varphi - \varphi_k)]\}. \end{aligned} \quad (8)$$

where

$$m_0 = \frac{\pi}{\delta\theta}, \quad J_0^{(i)} = \frac{m_0 I_d}{\pi r_{ci}}, \quad \theta_0 = \theta_1(0) - \delta\theta.$$

One can show that the current density (8) can be expanded into a Fourier series,

$$\vec{j}_i(r, \theta, \varphi) = 2\vec{e}^{(i)} \sum_{m=-\infty}^{\infty} \sum_{n=-\infty}^{\infty} \sum_{s=1}^{\infty} j_{mn}^{(si)}(r) \cos\left(m\theta - n\varphi + \chi_{mn}^{(s)}\right), \quad (9)$$

with the Fourier coefficients

$$j_{mn}^{(si)}(r) = (-1)^q \delta(r - r_{ci}) \tilde{J}_0^{(i)} C_n^{(s)} g_{mi}^{(s)},$$

$$\chi_s = m_0(2s - 1)\theta_0, \quad (10)$$

where

$$\tilde{j}_0^{(i)} = \frac{6J_0^{(i)} \Delta\varphi \Delta\theta_i}{(2\pi)^2} = \frac{m_0 I_d}{\pi r_{ci}} \frac{6\Delta\varphi \Delta\theta_i}{(2\pi)^2}, \quad (11)$$

$$g_{mi}^{(s)} = \frac{\sin([m - m_0(2s - 1)]\Delta\theta_i/2)}{[m - m_0(2s - 1)]\Delta\theta_i/2}, \quad (12)$$

$$C_n^{(s)} = \frac{\sin([n - m_0(2s - 1)\alpha]\Delta\varphi/2)}{[n - m_0(2s - 1)\alpha]\Delta\varphi/2}. \quad (13)$$

The toroidal mode number n takes values $n = 6q, q = 0, \pm 1, \pm 2, \dots$. As one can see from Eqs. (10) and (13), the biggest effect occurs when the ED coils are designed in such a way that the product $m_0\alpha$ is close to the toroidal mode $n_0 = 6$, i.e., $|m_0\alpha - n_0| \ll \Delta\varphi/2$. Then in the sum (9), the main contribution comes from the terms with the toroidal numbers $n = (2s - 1)n_0, (s = 1, 2, \dots)$. Leaving in Eq. (9) only these terms we have

$$\vec{j}_i(r, \theta, \varphi) = 2\vec{e}^{(i)} \sum_{m=-\infty}^{\infty} \sum_{s=1}^{\infty} j_{mn}^{(si)}(r) \times \cos(m\theta - (2s - 1)n_0\varphi + \chi_s), \quad (14)$$

where $n_0 = 6, i = 1, 2$.

2.2 Magnetic field in a cylindrical approximation

First we consider the magnetic field created by the helical currents (14). Using the procedure similar in Ref. [51] one can obtain the exact formula for the scalar potential $\Phi(r, \theta, \varphi)$. Then the perturbation magnetic field is given by $\mathbf{B}(r, \theta, \varphi) = \nabla\Phi(r, \theta, \varphi)$. For $r < r_{ci}, (i = 1, 2)$ one has

$$\begin{aligned} \Phi(r, \theta, \varphi) &= \Phi_1(r, \theta, \varphi) + \Phi_2(r, \theta, \varphi), \\ \Phi_i(r, \theta, \varphi) &= \sum_{m=-\infty}^{\infty} \sum_n \Phi_{mn}^{(i)}(r) \sin(m\theta - n\varphi + \chi_s), \end{aligned} \quad (15)$$

where $n = (2s - 1)n_0, (s = 1, 2, \dots)$ and

$$\begin{aligned} \Phi_{mn}^{(i)}(r) &= -B_c^{(i)} C_n^{(s)} g_m^{(si)} f_{mn}^{(i)}(r) \frac{r_{ci}}{m}, \\ f_{mn}^{(i)}(r) &= -\frac{2nr_{ci}}{R_{ci}} K_m' \left(\frac{nr_{ci}}{R_{ci}} \right) I_m \left(\frac{nr}{R_{ci}} \right), \\ B_c^{(i)} &= \frac{2\mu_0 m_0 I_d \cos(\alpha_{0i})}{\pi r_{ci}} \frac{6\Delta\varphi \Delta\theta_i}{(2\pi)^2}, \end{aligned} \quad (16)$$

where $I_m(z)$ and $K_m(z)$ are the modified Bessel functions ($K_m'(z) \equiv dK_m(z)/dz$).

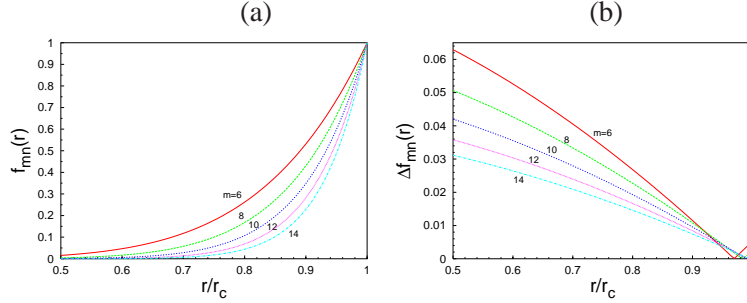


Figure 2: (a) Radial dependence of the function $f_{mn}(r)$ for different poloidal modes m . (b) Relative deviation of the $f_{mn}(r)$ from the power law $(r/r_c)^m$: $\Delta f_{mn}(r) = |f_{mn}(r) - (r/r_c)^m|/f_{mn}(r)$. Parameters are $r_c = 85$ cm, $R_0 = 238$ cm, $n = 6$.

Here $B_c^{(i)}$ is the characteristic amplitude of external magnetic field strength². For the typical parameters of the ED of Tore Supra ($r_c = 0.85$ m, $I_d = 22.5$ kA) we have $B_c \approx 425$ G. It is close to the value, $B_c \approx 405$ G, of the corresponding quantity for the TEXTOR-DED (at $I_d = 15$ kA).

The radial dependences of the perturbation field are described by functions $f_{mn}^{(i)}(r)$ which are shown in Fig. 2 for a several mode numbers m . For large mode number m ($m \geq 4$) the radial dependence is well described by the following asymptotical formula $f_{mn}^{(i)}(r) \approx (r/r_{ci})^m$. Then the radial component of the magnetic field B_r can be represented as

$$B_r(r, \theta, \varphi) = B_r^{(1)}(r, \theta, \varphi) + B_r^{(2)}(r, \theta, \varphi),$$

$$B_r^{(i)}(r, \theta, \varphi) = - \sum_{m=-\infty}^{\infty} \sum_{s=1}^{\infty} B_c^{(i)} C_n^{(s)} g_m^{(si)} \left(\frac{r}{r_{ci}} \right)^{m-1} \sin(m\theta - (2s-1)n_0\varphi + \chi_s).$$

2.3 Toroidal corrections

We consider the first order correction to the magnetic field perturbations due to toroidicity of the system. According to [56] this effect can be taken into account by multiplying the scalar potential $\Phi(r, \theta, \varphi)$ obtained in the cylindrical approximation with the factor $\sqrt{R_0/(R_0 + r \cos \theta)}$ when the corrections of order $(nr_c/2R_c)^m$ are small. In this case we have

$$\Phi(r, \theta, \varphi) = \sqrt{\frac{R_0}{R_0 + r \cos \theta}} [\Phi_1(r, \theta, \varphi) + \Phi_2(r, \theta, \varphi)], \quad (18)$$

where the functions $\Phi_i(r, \theta, \varphi)$, ($i = 1, 2$) are given by Eq. (15). We present the corresponding radial magnetic field as a sum of contributions corresponding to

²We should note that the definition of $B_c^{(i)}$ as well as coefficients $g_m^{(si)}$ are slightly different from the corresponding ones given in Ref. [48, 51]

different toroidal modes, n ,

$$B_r(r, \theta, \varphi) = \frac{\partial \Phi}{\partial r} = \sum_n B_r^{(n)}(r, \theta, \varphi), \quad (19)$$

$$B_r^{(n)}(r, \theta, \varphi) = \sum_{m=-\infty}^{\infty} B_{mn}(r, \theta) \sin(m\theta - n\varphi + \chi_s),$$

where

$$\begin{aligned} B_{mn}(r, \theta) &= \frac{\partial}{\partial r} \sqrt{\frac{R_0}{R_0 + r \cos \theta}} \left[\Phi_{mn}^{(1)}(r) + \Phi_{mn}^{(2)}(r) \right] \\ &= \left[B_c^{(1)} g_{m1}^{(s)} \left(\frac{r}{r_{c1}} \right)^{m-1} + B_c^{(2)} g_{m2}^{(s)} \left(\frac{r}{r_{c2}} \right)^{m-1} \right] \\ &\quad \times \sqrt{\frac{R_0}{R_0 + r \cos \theta}} \left(1 - \frac{r \cos \theta}{2m(R_0 + r \cos \theta)} \right). \end{aligned} \quad (20)$$

The toroidal component of the vector potential of the perturbation field takes the form

$$A_\varphi(r, \theta, \varphi) = \epsilon B_0 R_0 a(r, \theta, \varphi) = \epsilon B_0 R_0 \sum_{m=-\infty}^{\infty} \sum_n a_{mn}(r, \theta) \cos(m\theta - n\varphi + \chi_{mn}),$$

$$a_{mn}(r, \theta) = m^{-1} r B_{mn}(r, \theta), \quad (21)$$

where ϵ stands for the dimensionless perturbation parameter, defined as $\epsilon = B_c^{(1)}/B_0$, B_0 is the strength of the toroidal field. The dimensionless Fourier coefficients, $a_{mn}(r, \theta)$, are then given by

$$a_{mn}(r, \theta) = a_{mn}^{(1)}(r, \theta) + \delta a_{mn}^{(2)}(r, \theta), \quad (22)$$

where

$$\begin{aligned} a_{mn}^{(i)}(r, \theta) &= g_m^{(i)} \frac{r_{ci}}{mR_0} \frac{r}{m} \frac{d}{dr} \left(\sqrt{\frac{R_0}{R_0 + r \cos \theta}} \left(\frac{r}{r_{ci}} \right)^m \right) \\ &= g_{mi}^{(s)} \frac{r_{ci}}{mR_0} \left(\frac{r}{r_{ci}} \right)^m \sqrt{\frac{R_0}{R_0 + r \cos \theta}} \left(1 - \frac{r \cos \theta}{2m(R_0 + r \cos \theta)} \right) \end{aligned} \quad (23)$$

Here ($i = 1, 2$), $\delta = B_c^{(2)}/B_c^{(1)} = r_{c1}\Delta\theta_2/(r_{c2}\Delta\theta_1)$. The phase $\chi_{mn} = \chi_s$ and toroidal mode number $n = (2s - 1)n_0$.

The angular dependencies of the perturbation field $B_r(r, \theta, \varphi)$ at the fixed values of radial coordinate r and the toroidal angle $\varphi = 0$ are plotted in Fig. 3. The radial dependence of the perturbation field is determined by the poloidal mode

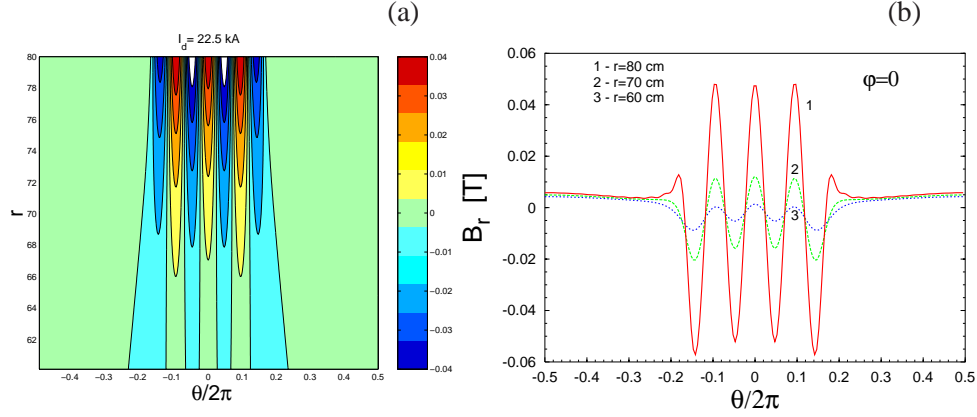


Figure 3: Radial component of the perturbation field B_r : (a) contour plot in the (θ, r) plane ($\varphi = 0$); (b) poloidal dependence at different radial positions r : 1 – $r=80$ cm, 2 – $r=70$ cm, 3 – $r=60$ cm. $I_d=22.5$ kA.

spectra, g_{mi} . According to the definition given by Eq. (12) the latter is localized near the central mode $m_c = (2s-1)m_0 = nm_0/n_0$, ($s = 1, 2, \dots$) and has a width $\Delta m = \pi/\Delta\theta_i$. Therefore, one expects that the perturbation field, $B_r^{(n)}(r, \theta, \varphi)$ of the n -th toroidal mode has the following radial dependence,

$$B_r^{(n)}(r, \theta, \varphi) \propto \left(\frac{r}{r_{ci}}\right)^{\gamma_n}, \quad \gamma_n = \frac{nm_0}{n_0} - 1. \quad (24)$$

The power law of the radial decay of perturbation field has the lowest exponent, $\gamma_{n=6} = m_0 - 1$, for the toroidal mode $n = 6$. For the value $\delta\theta = 18^\circ$, one has $m_0 = \pi/\delta\theta = 10$ the exponent $\gamma = 9$. For the next toroidal mode $n = 18$ we have $\gamma_{n=18} = 3m_0 - 1 = 29$.

It should be pointed out that the power-law decay of the perturbation field (24) found here is different from the exponential decay law $\exp(-m_0(r_{ci} - r)/r_{ci})$ proposed for the ED in Tore Supra [44].

2.4 Determination of the spectra of magnetic perturbation $H_{mn}(\psi)$

Starting from the expressions (19) to (23) for the perturbation field $B_r(r, \vartheta, \varphi)$ and the toroidal component of its vector potential, the field line structure in the Tore Supra ED edge can be studied following the approach described in [51]. In terms of magnetic flux coordinates $(\psi_{pol}, \psi \equiv \psi_{tor}, \vartheta, \varphi)$ the magnetic field \mathbf{B} can be presented in the Clebsch form [57–59], where (ψ_{pol}, ψ) are poloidal and toroidal fluxes, (ϑ, φ) are poloidal and toroidal angles. In this coordinate system the field line equations have the Hamiltonian form

$$\frac{d\psi}{d\varphi} = -\frac{\partial\psi_{pol}}{\partial\vartheta} \quad \frac{d\vartheta}{d\varphi} = \frac{\partial\psi_{pol}}{\partial\psi}, \quad (25)$$

with the Hamiltonian

$$\begin{aligned}
\psi_{pol} &= \psi_{pol}^{(0)}(\psi) + \psi_{pol}^{(1)}(\psi, \vartheta, \varphi), \\
\psi_{pol}^{(0)}(\psi) &= \int \frac{d\psi}{q(\psi)}, \\
\psi_{pol}^{(1)}(\psi, \vartheta, \varphi) &= \epsilon \sum_{m,n} H_{mn}(\psi) \cos(m\vartheta - n\varphi + \chi_{mn}). \tag{26}
\end{aligned}$$

where $q(\psi)$ is the safety factor of the equilibrium plasma, $H_{mn}(\psi)$ are the Fourier coefficients of the perturbation field corresponding to the poloidal mode numbers m and the toroidal mode n . The equations (25) are integrated using the computationally efficient mapping method (see Refs. ([52–54]).

The equilibrium plasma of the Tore Supra tokamak is modelled by a plasma with nested, circular magnetic surfaces with an outward (Shafranov) shift due to effects of the plasma pressure and electric current, again completely similar to the equilibrium plasma model described in [51] (which is based on expressions for the Shafranov shift, the toroidal current density profile of a cylindrical plasma model and the representation of the safety factor due to toroidicity as a series of powers of the inverse aspect ratio given in [44], [60] and [48], respectively). The ripple of the magnetic field was not yet incorporated in the modelling presented here, thus ruling out the possibility of a direct comparison of the results with experimental evidence.

In order to integrate the field line equations, the Fourier components $H_{mn}(\psi)$ of the perturbation Hamiltonian have to be determined. According to Refs. [48, 51, 54] those are found by the following Fourier integral from the product of the major radius $R = R_0 + r \cos \theta$ and the vector potential A_φ of the perturbation field (21),

$$H_{mn}(\psi) = \text{Re} \int_0^{2\pi} \int_0^{2\pi} \frac{RA_\varphi(r, \theta, \varphi)}{(2\pi)^2 B_0 R_0^2} e^{-im\vartheta + in\varphi} d\vartheta d\varphi, \tag{27}$$

where (r, θ) is the unperturbed field line on the given magnetic surface ψ and ϑ is the intrinsic poloidal angle which is different from the geometrical poloidal angle θ . In the Eq. (27) it is supposed that (r, θ) is a function of the ψ and ϑ : $r = r(\psi, \vartheta)$, $\theta = \theta(\psi, \vartheta)$.

Using the Fourier series in Eq. (21) the integral can be reduced to

$$\begin{aligned}
H_{mn}(\psi) &= \frac{1}{2\pi} \sum_{m'} \int_0^{2\pi} b_{m'n}(r, \theta) e^{-i[m\vartheta - m'\theta(\vartheta)]} d\vartheta, \\
b_{m'n}(r, \theta) &= a_{m'n}(r, \theta) \left(1 + \frac{r \cos \theta}{R_0}\right)^{1/2}. \tag{28}
\end{aligned}$$

As seen from Eq. (28) the toroidal spectra, n , of the perturbation field remain unchanged. However, the poloidal spectra, $b_{mn}(r, \theta)$, in the geometrical space,

(r, θ) , changes drastically in the (ψ, ϑ) space. First following Refs. [48, 51, 54] we qualitatively estimate the integral (28) in order to reveal the main features of the transformation of the spectra of magnetic perturbations.

The integral (28) contains the fast oscillating phase $f(\vartheta) = m\vartheta - m'\theta(\vartheta)$ and slowly varying amplitude $b_{m'n}(r, \theta)$. Therefore it can be estimated using asymptotical methods [61]. As was shown in [51, 54] for the perturbation field located on the low field side of the torus the $H_{mn}(\psi)$ is given by the following asymptotical formula

$$H_{mn}(\psi) = \sum_{m'} b_{m'n}(r, \theta = 0) \left(\frac{2}{|\gamma_3| m'} \right)^{1/3} \text{Ai} \left(-\frac{\gamma_1 m' - m}{(|\gamma_3| m'/2)^{1/3}} \right), \quad (29)$$

where the coefficients γ_1 and γ_3 are the first and third derivatives of the geometrical angle θ with respect to the intrinsic angle ϑ taken on the low field side of the torus, $\theta = 0$, respectively:

$$\gamma_1 = \left. \frac{d\theta}{d\vartheta} \right|_{\theta=0}, \quad \gamma_3 = \left. \frac{d^3\theta}{d\vartheta^3} \right|_{\theta=0}. \quad (30)$$

We should note that $\gamma_1 > 1$, $\gamma_3 < 0$, and their particular values depend on the equilibrium plasma configuration. The sum (29) can be replaced by integration over m' and asymptotically estimated. This procedure gives

$$H_{mn}(\psi) \approx \gamma_1^{-1} B b_{m'(m)n}(r, \pi = 0), \quad (31)$$

where $m'(m)$ is determined by

$$m'(m) = \frac{m - x_c (|\gamma_3| m/2)^{1/3}}{\gamma_1}, \quad (32)$$

and $B = \sqrt{2\pi/|x_c|} \text{Ai}(x_c)$, and $x_c \approx -1$ is the local maximum of the Airy function.

The obtained relation (31) describes the transformation law of the poloidal spectra of magnetic perturbations in a geometrical space to the ones in intrinsic coordinates. As was mentioned above the poloidal mode spectra a_{mn} at the given toroidal mode n are localized near the central mode $m_c = nm_0/n_0$ with a poloidal mode extension $\Delta m = \pi/\Delta\theta_i$. Then from Eqs. (31), (32) it follows that the spectrum, H_{mn} , has the same form as a_{mn} , but its central mode m_c^* is shifted to the higher number $m_c^* \approx m_c \gamma_1$ and the width becomes larger $\Delta m^* \approx \Delta m \gamma_1$, since $\gamma_1 > 1$. These rigorously obtained results coincide with the corresponding ones obtained in [44, 55] by a qualitative analysis.

However, the radial dependence of perturbation modes $H_{mn}(\psi)$ (31) has a power-law $H_{mn}(\psi) \propto r^{m/\gamma_1}$ in contrast to the exponential law $\exp(-m(r_c - r)/r_c)$ supposed in [44, 45].

The mode transformation is illustrated in Fig. 4 where the comparison of the asymptotical formula (31), (32) for $H_{mn}(\psi)$ (curve 2) with its numerically calculated value (curve 3) from the integral (28) is shown. Parameters B and x_c in the

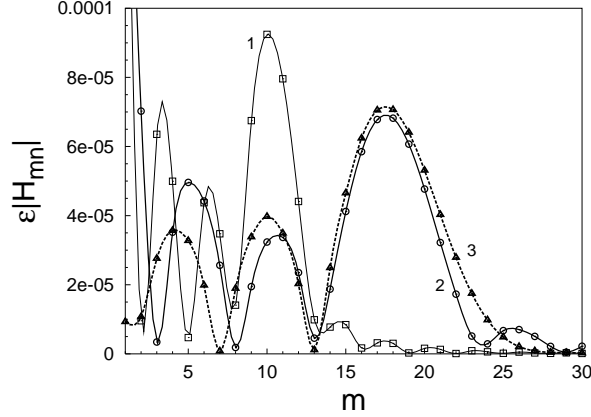


Figure 4: Poloidal spectra of magnetic perturbation field at the magnetic surface $q = 3$: Curve 1 describes $b_m(r, 0)$, curve 2 corresponds to the asymptotical formula (31), (32) with the fitting parameters $B = 1.4$, $x_c = -0.5$, and curve 3 corresponds to the numerical calculations of the integral (28). The plasma parameters are the plasma minor radius $a = 80$ cm, the major radius $R_0 = 238$ cm, the toroidal field $B_t = 3.03$ T, the plasma current $I_p = 1.5$ MA, the plasma $\beta_{pol} = 0.13$. The ED current $I_d = 22.5$ kA, $\delta\theta = 19^\circ$, $\Delta\varphi = \pi/14$. The quantities $\gamma_1 = 1.85$, $\gamma_3 = -3.124$.

asymptotical formula are considered as fitting parameters. Curve 1 corresponds to the spectra $b_m(r, 0)$ in the geometrical space. As seen from Fig. 4 the asymptotical formula describes well the transformation law of the poloidal spectra of magnetic perturbations.

The asymptotical formula (31) resulting from the qualitative analysis of the transformation of perturbation modes in geometrical coordinates to the ones in flux coordinates is important, as it contributes to understanding the features of mode transformations in toroidal systems and clearly shows the differences between the cases when the perturbation coils are located on the low-field-side (for the ED of Tore Supra) and on the high-field side (the TEXTOR-DED, for which the corresponding formula is given in Sect. 2.5), without having to resort to numerical computations.

Fig. 5 shows the contour plot of the poloidal spectra of magnetic perturbations $H_{mn}(\psi)$ for the toroidal modes $n = 6$ and $n = 18$, respectively. The values $H_{mn}(\psi)$ at the resonant surfaces ρ_{mn} (or ψ_{mn} , $nq(\psi_{mn}) = m$) lie at the white curve $nq(\rho)$. One can see that the magnetic perturbation have a wide spectrum with the central modes $m_c^*(\psi_{mn})$ at the rational magnetic surface ψ_{mn} , ($q(\psi_{mn}) = m/n$) close to the corresponding resonant mode numbers m . It covers the rational magnetic surfaces located at the plasma edge between $q \geq 2$ and $q = 3.5$. The magnetic perturbation for the toroidal mode $n = 18$ is one order smaller than for the mode $n = 6$.

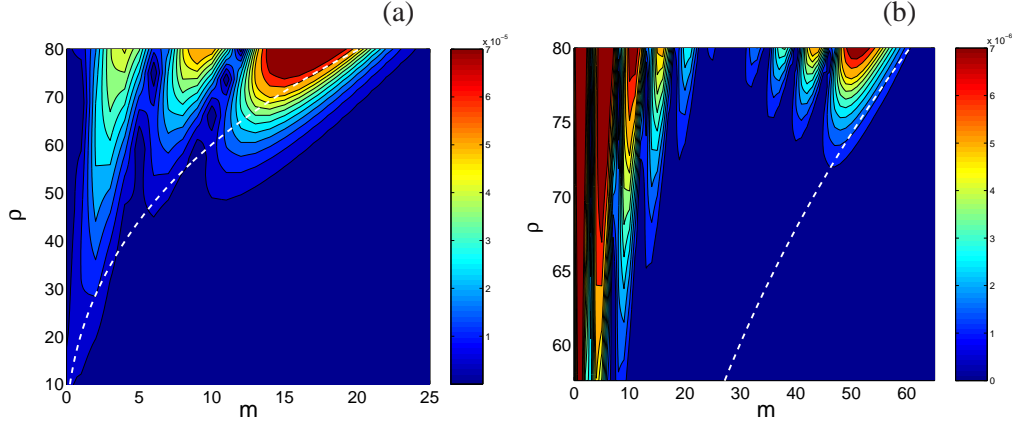


Figure 5: (a) Contour plot of poloidal spectrum of perturbation field, $\epsilon|H_{mn}|$, in the (m, ρ) – plane for the toroidal mode $n = 6$. White dashed curve corresponds resonant line $(nq(\rho), \rho)$. (b) The same as in (a) but for the toroidal mode $n = 18$. Parameters are the same as in Fig. 4.

The resonant components of $H_{mn}(\psi_{mn})$ decay inwardly as $H_{mn}(\psi_{mn}) \propto \psi_{mn}^{m_r/2}$, with $m_r \approx 7.9$ for the toroidal mode $n = 6$.

2.5 Comparison with the TEXTOR-DED

Unlike the ED coils in Tore Supra, the perturbation coils of the DED of TEXTOR are located on the high-field-side (HFS) of the torus [48, 49, 51, 62]. It consists of 16 helical coils continuously winding around the torus with the poloidal extension, $\Delta\theta \approx 72^\circ$. By special arrangement of the current distribution over the coils one can create the perturbation field with the dominant toroidal modes, $n = 4$, $n = 2$, and $n = 1$, which are called $m : n = 12:4$, $6:2$, and $3:1$ operational modes, respectively. The poloidal spectrum, $|b_{mn}(r, \theta)|$, of the perturbation field in the geometrical space has a wide spectrum with the central mode $m_c = nm_0/4 \approx 5n$ and the width $\Delta m \approx \pi/\Delta\theta$, where $m_0 \approx 20$. It is shown as curve 1 in Fig. 6 for the toroidal mode $n = 4$. The radial decay of the modes $|b_{mn}|$ has a power law $|b_{mn}(r, \theta)| \propto (r/r_c)^m$, and correspondingly the full radial perturbation magnetic field, $B_r \propto (r/r_c)^{\gamma_n}$, with the exponent, $\gamma_n \approx m_0 - 1 = 19$, which is twice larger than the corresponding exponent γ_n for the ED of Tore Supra (see Eq. (24)). It means that the perturbation field in the TEXTOR-DED does not penetrate into the plasma much deeper than in the case of the ED of Tore Supra.

On the other hand the transformation from geometrical to intrinsic coordinates for the TEXTOR-DED case, modifies the perturbation field spectrum, $\epsilon|H_{mn}|$, in a completely different way. An example of this spectrum is shown in Fig. 6 as curve 2. The central mode number m_0 of the poloidal spectrum in the geometrical space is about $m_0 \approx 20$ and the width $\Delta m \approx 10$. In intrinsic coordinate the central mode is shifted to $m_0^* \approx 12$, and the width $\Delta m^* \approx 6$.

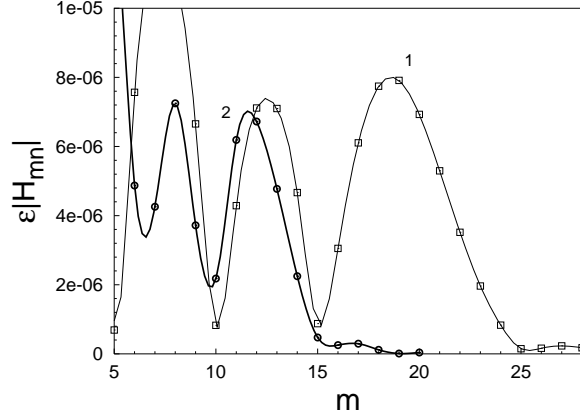


Figure 6: Typical poloidal spectrum of perturbation field $\epsilon|H_{mn}|$ at the magnetic surfaces $q = 3$ in the TEXTOR-DED: curve 1 describes $b_m(r, \pi)$, curve 2 corresponds to numerically calculated $H_{mn}(\psi)$. Parameters of the plasma are $B_t = 1.9$ T, $I_p = 382$ kA, $\beta_{pol} = 0.5$, $a = 44.7$ cm, $R_0 = 175$ cm, the DED current, $I_d=15$ kA.

As was shown in Refs. [48,49,51] this spectrum has the following asymptotics

$$H_{mn}(\psi) \approx (-1)^m \beta_1^{-1} B b_{m'(m)n}(r, \pi = \pi),$$

$$m'(m) = \frac{m + x_c (\beta_3 |m/2|)^{1/3}}{\beta_1}, \quad (33)$$

where β_1 and β_3 are the first and the third derivatives of θ with respect to ϑ taken on the high field side $\vartheta = \pi$ [51,54]. We note that $\beta_1 < 1$. In this case the central mode m_c^* is shifted to the lower mode number $m_c^* = m_c \beta_1$, and the width of the spectra is decreased, $\Delta m^* \approx \Delta m \beta_1$.

Thus the analytical analysis made in Secs. 2.4 and 2.5 show that the effect of the perturbation significantly changes when the coils are moved from one side of the torus to the opposite one. If the TEXTOR-DED coils were located on the low-field-side with the same coil design the effect of the perturbation would be drastically increased: the group of modes of b_m centered near $m_c \approx 20$ would be transferred to the mode group with the central mode number $m_c^* \approx \gamma m_c \approx 36$ and the width $\Delta m^* \approx \gamma \Delta m \approx 18$ which however are not resonant at the plasma edge. The resonant modes of H_{mn} with $m \approx 10 - 14$ would be formed from the group of modes of b'_m with $m' = 5 - 8$. The radial decay of these modes is much weaker, i.e., $H_{mn} \propto r^\gamma$, ($\gamma = 5 - 8$), and they penetrate much deeper into the plasma. In the case of Tore Supra the move of the ED coils to the opposite side would significantly weaken the effect of perturbation. The resonant modes H_{mn} with $m = 14 - 20$ will be formed from the group of modes of b'_m with $m' \approx 25 - 33$, which has a much stronger radial decay $H_{mn} \propto r^\gamma$, ($\gamma = 25 - 33$).

In reality the coils for the Tore Supra ED as well as the TEXTOR-DED are

designed to have a group of modes near the central mode perturbation, m_c^* , which are resonant to field lines near the $q = 3$ surface of the plasma edge.

In addition, from Eqs. (31) and (33) the following roughly determined radial decay laws for the perturbation modes can be derived: $H_{mn}(\psi) \propto r^{m/\gamma_1}$, ($\gamma_1 > 1$) for the ED of Tore Supra and $H_{mn}(\psi) \propto r^{m/\beta_1}$, ($\beta_1 < 1$) for the TEXTOR-DED, i.e., in the first case at a given poloidal mode m , the radially inward decay of the perturbation is much weaker than in the second case. This is most probably related to the location of perturbation coils on the low-field-side and the high-field-side, respectively, although differences in design between the perturbation coils in Tore Supra ED and TEXTOR-DED can not completely be ruled out as a possible explanation.

3 Structure and statistical properties of the ergodic zone

3.1 Qualitative estimates of the formation of the ergodic zone at the plasma edge

Similarly to the analysis which has been made for TEXTOR-DED [51], a qualitative picture of the formation of the ergodic zone in Tore Supra ED can be obtained by considering the Chirikov parameter [63,64], which is determined by the perturbation spectrum and the $q(\rho)$ -profile.

This Chirikov parameter, σ_{Chir} , as a function of the mean radius of the neighboring resonant magnetic surfaces, $\rho = (\rho_{m+1,n} + \rho_{mn})/2$, is shown in Fig. 7 for the three different perturbation currents: $I_d = 4.5$ kA (curve 1), $I_d = 9$ kA (curve 2), and $I_d = 22.5$ kA (curve 3). As seen from Fig. 7 the Chirikov parameter, σ_{Chir} ,

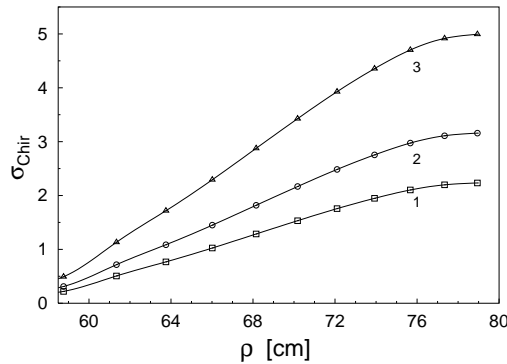


Figure 7: Chirikov parameter σ_{Chir} vs the radial coordinate ρ for the different perturbation currents: curve 1 corresponds $I_d = 4.5$ kA, curve 2 – $I_d = 9$ kA, and curve 3 – $I_d = 22.5$ kA. The plasma parameters are the same as in Fig. 4.

grows linearly with the radius, ρ , and exceeds the unity (which is the criterium for the overlapping of magnetic islands) at $\rho > \rho_1 \approx 66$ cm for the perturbation current $I_d = 4.5$ kA, $\rho > \rho_2 \approx 64$ cm for $I_d = 9$ kA, and $\rho > \rho_3 \approx 61$ cm

for $I_d = 22.5$ kA. Therefore, the field lines are chaotic in the regions, $\rho > \rho_i$, ($i = 1, 2, 3$), at the corresponding perturbation currents, $I_d = 4.5$ kA, $I_d = 9$ kA, and $I_d = 22.5$ kA, respectively.

3.2 Structure of the ergodic zone

A more precise picture of the onset of chaotic field lines and the formation of the ergodic zone can be obtained by Poincaré sections and laminar plots of field lines. Below we construct these plots employing the earlier mentioned mapping method of integration of field line equations. Furthermore, the integration step, $\Delta\varphi$, of the mapping along the toroidal angle φ , is chosen equal to $2\pi/ns$, with $n = 6$ and $s = 4$.

In Figs. 8a-c Poincaré sections of field lines in the poloidal plane $\varphi = 0$ are plotted for the three different perturbation currents, I_d : (a) $I_d = 4.5$ kA, (b) $I_d = 9$ kA, and (c) $I_d = 22.5$ kA for the plasma and ED parameters corresponding to the spectrum of magnetic perturbations shown in Fig. 4. We plotted Poincaré sections in the (ρ, ϑ) plane which clearly reveal the positions of the magnetic surfaces. (In this plane the unperturbed field lines are presented by straight lines, $\rho = \text{const}$).

We can see from Fig. 8a that even at the lower level perturbation current $I_d=4.5$ kA one obtains a rather highly-developed ergodic zone in the radial region $\rho > \rho_c \approx 63$ cm with open field lines to the plasma wall. It is formed by the overlap of nine primary neighboring magnetic islands with the poloidal mode numbers from $m = 11$ to $m = 19$ and the toroidal mode $n = 6$. There are only two remnants of KAM-stability islands near the boundary of the ergodic zone with the last intact magnetic surface $\rho_c \approx 63$ cm. In the radial direction the ergodization level increases and the remnants of KAM islands drastically shrink in size. The region of field lines with short wall to wall connection lengths (white areas in the Poincaré plots) grows when one approaches the plasma edge $\rho = 80$ cm. This area is known as a laminar zone.

With increasing perturbation current I_d the ergodic zone grows radially inward. At the same time the radial width of the laminar zone increases (see Fig. 8b,c). At the maximal perturbation current $I_d=22.5$ kA the magnetic island $m = 10, n = 6$ is overlapped to the ergodic zone and the radial extension of the laminar zone becomes $\Delta\rho_l \approx 12$ cm. (A more precise way of estimating the laminar zone boundary will be given in Sect. 3.5.1 using the radial dependence of the field line diffusion coefficients).

The magnetic field lines in the ergodic divertor are a typical example of an open chaotic scattering system and it is characterized by a certain (fractal) structure, especially, in the laminar zone (see, e.g., [51, 65]). The structure of the latter can be more clearly visualized by the so-called laminar plots, i.e., the contour plots of field line wall to wall connection lengths. Such a plot of connection lengths measured in poloidal turns is shown in Figs. 9a,b in the (ϑ, ρ) plane at the maximal perturbation current $I_d=22.5$ kA: (a) shows the plot in the whole poloidal section and (b) shows the expanded view of the rectangular area at the low-field-side (LFS)

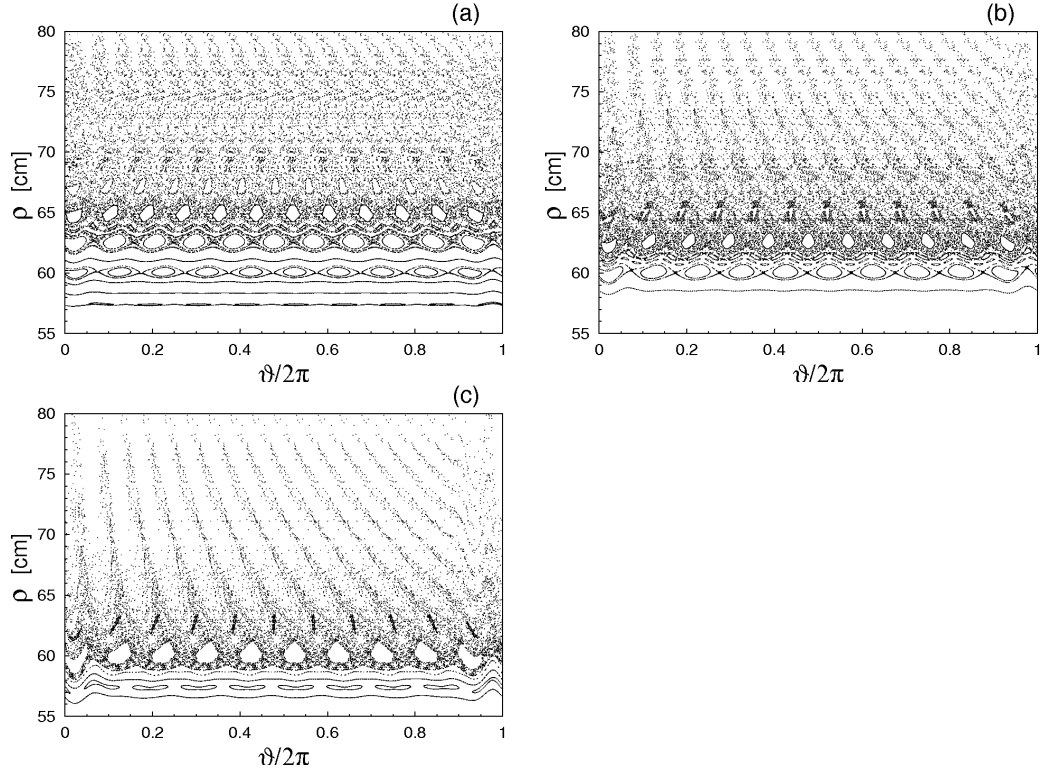


Figure 8: Poincaré sections of field lines in the (ϑ, ρ) plane at the three different perturbation currents: (a) – $I_d = 4.5$ kA, (b) – $I_d = 9$ kA, and (c) – $I_d = 22.5$ kA. The toroidal modes $n = 18$ beside the main mode $n = 6$ is taken into account into account. The plasma parameters are the same as in Fig. 4.

shown in (a). The corresponding Poincaré section was shown in Fig. 8c.

As seen from this figure the laminar zone forms a regular lattice-like structure in the large poloidal extended area, except the region on the LFS where field lines are distorted because of the magnetic perturbation which is localized on this side of the torus. One notices that the light blue “cells” in the laminar plot which correspond to the regions of field lines with wall to wall connection length of one poloidal turn are regularly located along the poloidal and radial directions. They are positioned between the resonant radii, ρ_{mn} . Their number along the poloidal direction at the given radius, ρ , coincides with the poloidal mode number, m , of the resonant radius, ρ_{mn} , located below the “cells”. The sizes of the “cells” grow with increasing radius ρ .

The expanded view of the laminar plot at the LFS shows also the so-called private flux zone (dark blue areas) of field lines which do not enter into plasma. Field lines coming from the inner regions of the plasma are connected to the wall along the elongated stripes (they are seen as black stripes).

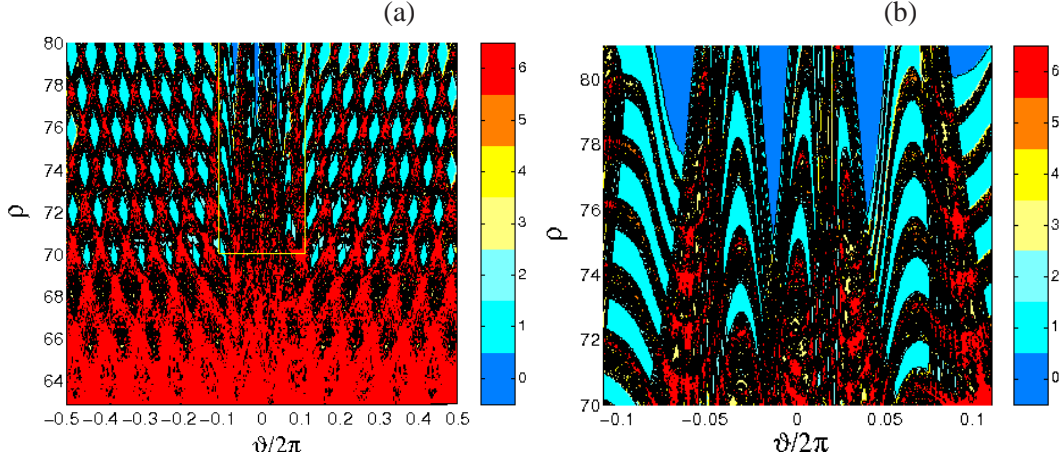


Figure 9: Laminar plots of field lines in the (ϑ, ρ) plane at the maximal perturbation current $I_d = 22.5$ kA corresponding to Fig. 8 c: (a) on the whole plane; (b) shows the expanded view of the rectangular area in (a).

3.3 Comparison with the TEXTOR-DED

As seen from the spectra of the magnetic perturbation, H_{mn} shown in Fig. 6 the ergodic zone at the plasma edge in the TEXTOR-DED is formed by the interaction of only a few poloidal modes, $11 \leq m \leq 14$, (12:4 operational mode) in contrast to the ED of Tore Supra ($11 \leq m \leq 20$). On the other hand, in TEXTOR-DED the magnetic perturbation radial decay has a power-law dependence with the exponent γ twice as large as in the ED of Tore Supra. Because of that one obtains in normal TEXTOR discharges an ergodized zone of field lines which are weakly connected to the wall. In order to increase the magnetic flux due to the perturbation field the plasma column is shifted to the HFS from the center of the torus.

An example of the ergodic zone when the plasma center is shifted over 3 cm from the center of the torus into the direction of the perturbation coils is shown in Fig. 10 where the Poincaré section and the laminar plot of field lines are displayed. The plasma parameters correspond to the discharge #93100: $I_p = 382$ kA, $B_t = 1.9$ T, $\beta_{pol} = 0.5$.

As seen from Fig. 10 in this shot the region of the stochastic field lines mostly consists of laminar zone with short wall to wall connection lengths. The width of the laminar zone is radially increased in expense of the ergodic zone of field lines with long connection lengths.

3.4 Magnetic footprints

Heat and particle deposition patterns on the divertor target plates are closely linked to the magnetic footprints on the corresponding plates. Since the geometry of divertor plates of Tore Supra is rather complicated, and in order to simplify the

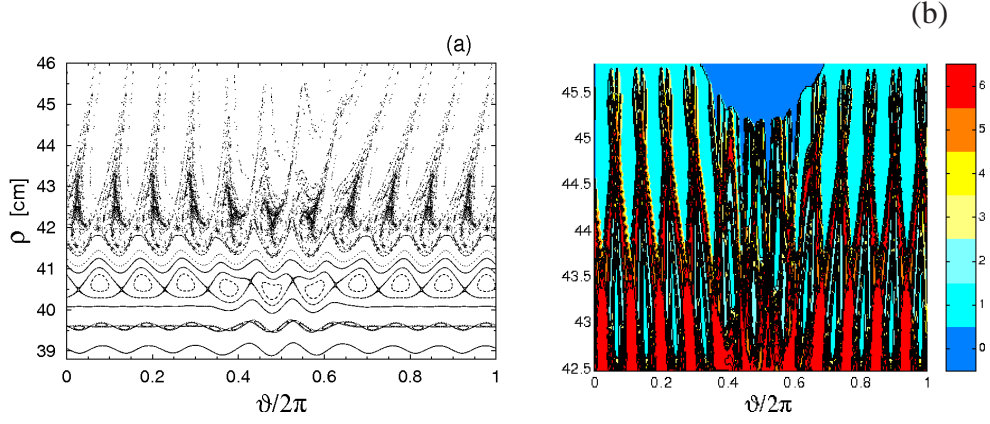


Figure 10: Poincaré section (a) and laminar plots (b) of field lines in the (ϑ, ρ) plane for the TEXTOR-DED. The plasma parameters are the same as in Fig. 6. The perturbation current $I_d = 7$ kA.

problem we study in a first approach the structure of magnetic footprints on the imaginary divertor plate at the minor radius $r_d = 80$ cm. We present them as contour plots of the wall to wall connection lengths measured in poloidal turns on the surface of $r_d = 80$ cm. The procedure of corresponding calculations is described in Refs. [51].

Such a plot of magnetic footprints is given in Fig. 11 for the same plasma and ED current parameters as in Fig. 8 c. Fig. 11a describes the magnetic footprints on the whole toroidal surface $r_d = 80$ cm, and (b) shows an expanded view of the region $0 < \varphi < 60^\circ$, $-120^\circ < \theta < 120^\circ$. As seen from these figures the footprints consists of $n = 6$ helical stripes corresponding to the toroidal mode number n as in the case of the TEXTOR-DED. Field lines coming from the inner plasma region hit the divertor plate along these helical stripes. Dark blue areas correspond to the private flux zone from which field lines cannot penetrate into the plasma.

If, in a more detailed approach, we take the exact geometry of the Tore Supra divertor plates into account, we need to adjust for two different aspects. Firstly, we need to modify the criterium used to determine if field lines hit the wall after each map step. Secondly, the radius r of the field line mapping starting positions on the ED module surfaces, will be a function of the toroidal and poloidal angle. A footprint plot in the (ϕ, θ) - plane taking those calculation procedure modifications into account, has been made for ED module 1 as a whole (shown in Fig. 11c) and, with higher resolution, for neutralizer 4 of the same module (Fig. 11d). On Fig. 11c the edges of the neutralizer plates have been indicated and the neutralizer plates have been numbered. On Fig. 11d we notice the pattern of helical stripes of higher connection length. The bended form of those stripes is due to the projection on the ϕ, θ - plane of the spatial structure of the neutralizer surface. It is clearly visible that, analogously to what was found for TEXTOR-DED [65], the helical stripes exhibit a fractal structure, i.e. self-similarity at different spatial scales.

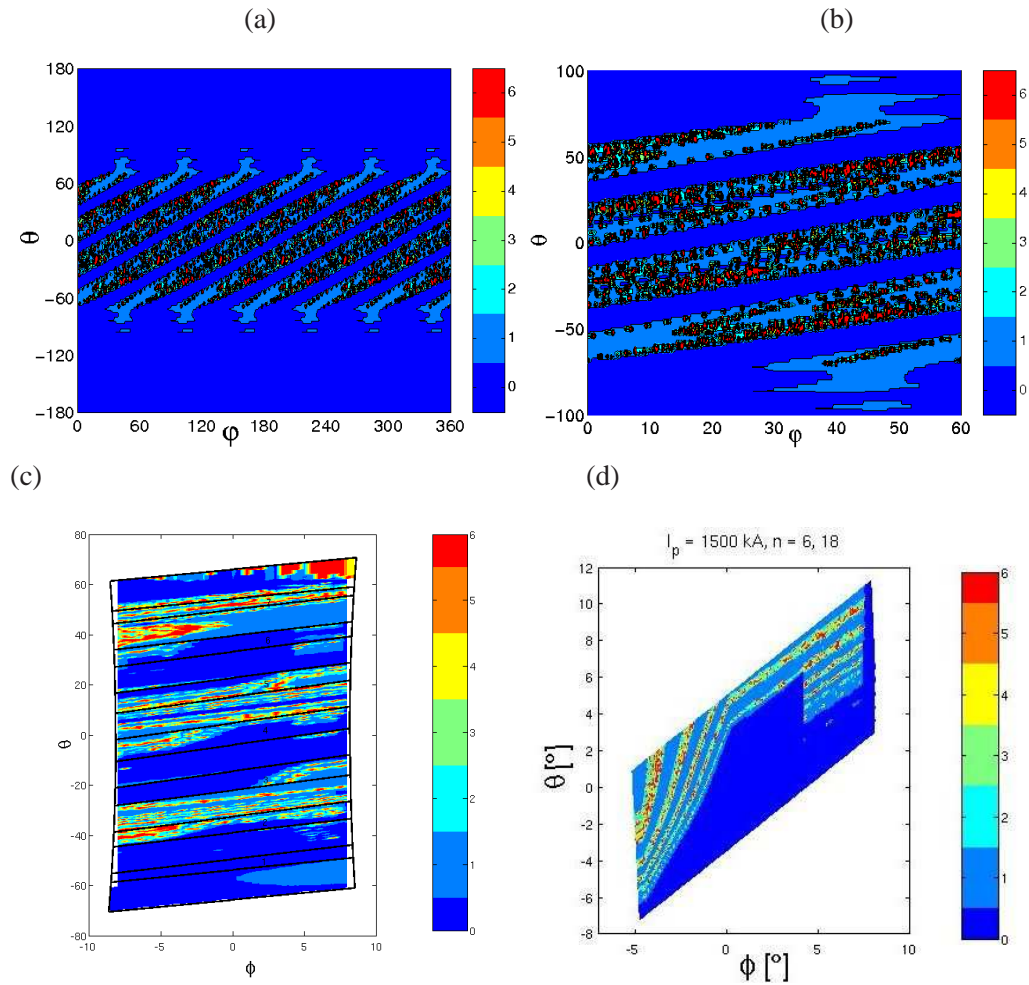


Figure 11: Contour plots of wall to wall connection lengths (magnetic footprints) of field lines in the imaginary divertor plate $r_d = 80$ cm. The perturbation current $I_d = 22.5$ corresponding to Fig. 8 c: (a) on the whole plane; (b) shows the expanded view of the region $0 < \varphi < 60^\circ$, $-120^\circ < \theta < 120^\circ$. (c) footprint plots on the surface of real divertor plate for ED module 1; (d) an expanded view of the above picture on the neutralizer 4.

3.5 Statistical properties of field lines

In order to estimate the level of radial heat and particles transport induced by the chaotic field lines one should estimate the statistical characteristics of those field lines. More precisely, one should study the radial diffusion coefficients of those field lines and the Kolmogorov lengths which characterize the degree of divergence of neighboring field lines. Below we calculate these statistical characteristics and compare them with their quasilinear estimations. For this we will follow the corresponding procedure described in Ref. [51].

3.5.1 Diffusion of field lines

Consider the second moment of the radial displacement of field lines,

$$\sigma^2(l) = \frac{1}{N} \sum_{i=1}^N (\rho_i(l) - \langle \rho(l) \rangle)^2, \quad (34)$$

where $l = R_0\varphi$ is a length of field lines. Averaging in (34) is performed over a number N of field lines uniformly distributed at the initial $\varphi = 0$ plane on the given magnetic of radius ρ . The local radial diffusion coefficient, D_{FL} , is defined as

$$D_{FL}(\rho) = \sigma^2(l)/2l,$$

at the initial linear growth regime $\sigma^2(l)$, as illustrated in Fig. 12. The diffusion

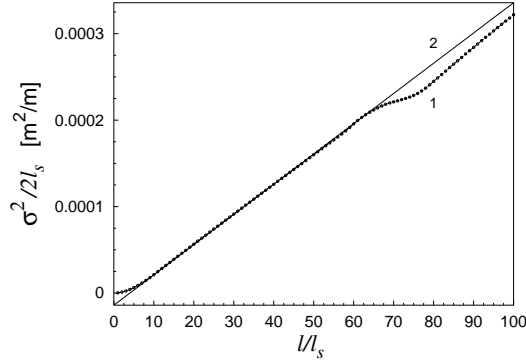


Figure 12: Determination of a local diffusion coefficient, D_{FL} , from the linear part of the dependence of the second moment of the radial displacement, $\sigma^2(\rho)$, of field lines on their length: curve 1 corresponds to $\sigma^2(\rho)/2l_s$, vs l/l_s ; curve 2 describes the linear curve $D_{FL}l/l_s$. Here l_s is a length of a field line per one map step.

coefficient determined in this way will be a local function of radius ρ .

Diffusion of field lines in the highly developed ergodized zone can also be estimated in the frame of quasilinear theory. One can show (see, [66,67]) that for

the Hamiltonian system of field lines mentioned in 2.4 and extensively described in [51] the distribution function, $f(\psi)$, of field lines along the toroidal flux, ψ is described by the Fokker-Planck equation

$$\frac{\partial f(\psi)}{\partial \varphi} = \frac{\partial}{\partial \psi} \left(D_M(\psi) \frac{\partial f(\psi)}{\partial \psi} \right), \quad (35)$$

where the diffusion coefficient $D_M(\psi)$ is given by the quasilinear formula³

$$D_M(\psi) = \frac{1}{2} \pi \epsilon^2 \sum_m |m H_{mn}|^2 \delta \left(\frac{m}{q(\psi)} - n \right). \quad (36)$$

The diffusion coefficient, $D_Q(\rho)$, along the radial coordinate, ρ , is related to $D_M(\psi)$ as

$$D_Q(\rho) = (R_0^3 / \rho^2) D_M(\psi), \quad (37)$$

The radial dependencies of the diffusion coefficients⁴, $D_{FL}(\rho)$, numerically calculated from the field line equations and the corresponding quasilinear diffusion coefficients, $D_Q(\rho)$ for the three different perturbation currents, I_d , are displayed in Fig. 13: $I_d = 4.5$ kA (curves 1 and 4), $I_d = 9.0$ kA (curves 2 and 5), and $I_d = 22.5$ kA (curves 3 and 6), (solid curves 1–3 describe $D_{FL}(\rho)$ and dashed curves 4–6 – $D_Q(\rho)$). The corresponding radial profiles of the averaged field line connection lengths are shown in Fig. 14. Again, the averaging was performed over a number N of field lines uniformly distributed at the initial $\varphi = 0$ plane on the given magnetic of radius ρ .

One sees from Fig. 13 that the numerically calculated diffusion coefficients, D_{FL} , steadily grow in certain radial regions, $\rho_{min} < \rho < \rho_l$. Close examination of the corresponding Poincaré sections given in Figs. 8 and the averaged connection lengths shown in Fig. 14 indicates that these radial regions correspond to the highly developed ergodic zone of field lines possessing the long connection lengths with its lower boundary at ρ_{min} and its boundary with the laminar zone at ρ_l . However, starting from ρ_l , the numerical diffusion coefficients, D_{FL} , stop to grow and abruptly go down, while the quasilinear diffusion coefficients, $D_Q(\rho)$, still continue to increase. The radius, ρ_l , can be called as the lower boundary of the laminar zone. As seen from Fig. 14 in the laminar zone $\rho > \rho_l$ the field lines have rather short connection lengths.

It is remarkable that for the smaller perturbation currents, $I_d = 4.5, 9$ kA, the numerical *diffusion coefficients*, D_{FL} , *perfectly follow the quasilinear formula (37) in the ergodic zones of field lines with long connection lengths*. However, they sharply deviate in the laminar zone with the short connection lengths. This contrasts with the radial profiles of diffusion coefficients presented in [51] for the case

³Note that the factor 1/2 in the definition of the quasilinear diffusion coefficient given in Ref. [66] is absent. This factor is included into the diffusion equation.

⁴The formulas (36), (37) for the diffusion coefficient are given in a singular form. Their actual values should be taken at the resonant values of $\rho = \rho_{mn}$ (or $\psi = \psi_{mn}$): $D_M(\psi_{mn}) = (1/2) \pi \epsilon^2 q(\psi_{mn}) m^2 |H_{mn}(\psi_{mn})|^2$.

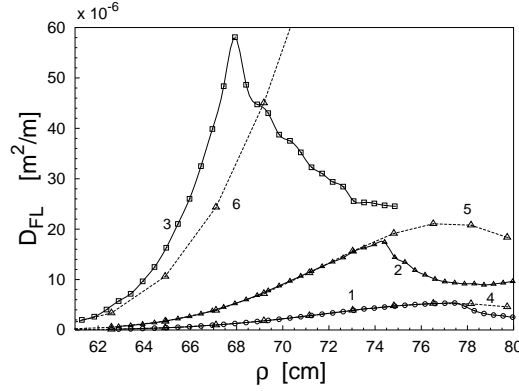


Figure 13: Radial dependencies of local field line diffusion coefficients, D_{FL} , of field lines at the three different perturbation currents: curves 1 and 4 correspond to $I_d = 4.5$ kA, curves 2 and 5 – $I_d = 9$ kA, and curves 3 and 6 – $I_d = 22.5$ kA. Solid curves 1–3 describe the numerical calculations and dashed curves 4–6 describe the quasilinear values, D_Q .

of the TEXTOR-DED 12:4 operational mode, where the correspondence between numerical and quasilinear diffusion coefficients in the ergodic zone is significantly worse. This difference might be explained by noticing that for the latter case, the applicability of the quasilinear theory is seriously hampered because the ergodic zone is formed by the overlap of only a few neighboring magnetic islands. In the ED Tore Supra case, on the contrary, a higher number of resonances, located closer to each other and thus showing a larger degree of overlap, result in a much better developed ergodic zone.

On the other hand, for the maximum perturbation current $I_d = 22.5$ kA the situation is different. The difference between the numerical D_{FL} and the quasilinear diffusion coefficient monotonically increases with the radius already in the ergodic zone, and the numerical $D_{FL}(\rho)$ exceeds $D_Q(\rho)$. The reason for such behavior of the $D_{FL}(\rho)$ is not clear yet and has to be investigated. A first indication might be given by the Poincaré section of Fig. 8 (c), where the ergodic character of the radial region just inward of ρ_l seems to be less pronounced than in the cases with the smaller perturbation currents. This suggests the existence of some additional averaged outward drift, due to a deeper reaching and dominating laminar zone.

In the case of the TEXTOR-DED the comparison of the numerical $D_{FL}(\rho)$ with the quasilinear diffusion coefficients, $D_Q(\rho)$, is not quite justified because the ergodic zone in the DED is formed by the interaction of only three or four magnetic islands. The quasilinear theory of diffusion can hardly be applied to such an ergodic zone. Particularly, for the case shown in Fig. 10 the numerical diffusion coefficient $D_{FL}(\rho)$ reaches the maximal value 3.7×10^{-6} m²/m at $\rho = 42.95$ cm, while its quasilinear value is 4.74×10^{-5} m²/m at the same radius, i.e., the quasilinear formula overestimates the diffusion coefficient by a factor 10.

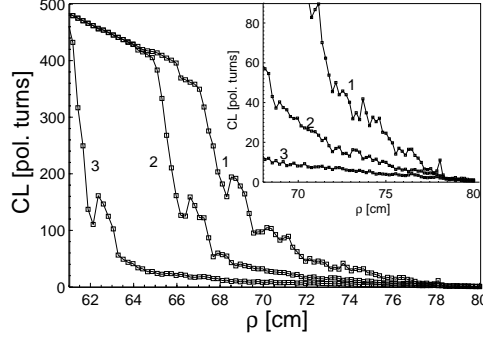


Figure 14: Radial dependence of the averaged field line connection length, measured in poloidal turns, at the three different perturbation currents: curve 1 corresponds to $I_d = 4.5$ kA, curve 2 – $I_d = 9$ kA, and curve 3 – $I_d = 22.5$ kA. The region nearest to the plasma edge has been enlarged in the upper right corner.

3.5.2 Kolmogorov lengths

The Kolmogorov time is a statistical characteristic of dynamical chaotic systems which characterizes the time of loss of information on initial state of the system. For chaotic field lines it corresponds to the characteristic decay length of the correlation of neighboring field lines, and called the Kolmogorov length. The calculation of the latter is based on the estimations of the Lyapunov exponents.

The numerical procedure of finding Kolmogorov lengths, L_K , for the chaotic field lines in the ergodic divertor is described in [51, 68]. It is based on the determination of the local Lyapunov exponents, $\sigma(\rho)$, describing the degree of exponential divergency of chaotic field lines launched from a given magnetic surface of radius ρ . The Kolmogorov length, L_K , is inverse proportional to $\sigma(\rho)$ averaged over the given magnetic surface, i.e., $L_K = 1/\bar{\sigma}(\rho)$.

The analytical formula for the Kolmogorov length, L_K , has been proposed by Ghendrih et al. [?], which expresses L_{KQ} , through the Chirikov parameter,

$$L_{KQ} = \pi q R_0 (\pi \sigma_{Chir}/2)^{-4/3}. \quad (38)$$

The numerically calculated radial profiles of L_K for the chaotic field lines in the ED of Tore Supra are shown in Fig. 15a for the three perturbation currents: curve 1 corresponds to $I_d = 4.5$ kA, curve 2 – $I_d = 9$ kA and curve 3 – 22.5 kA. The corresponding profiles of the analytical formula (38) are shown in Fig. 15b. The numerically calculated Kolmogorov length, L_K , is of the order of the connection length, $L_c = 2\pi q R_0$, which equal 44.9 m at the $q = 3$ magnetic surface. However, a comparison of Fig. 15a and b shows that the numerical Kolmogorov length exceeds the analytical estimation (38) by factors between five or ten. This discrepancy is probably related to the approximate character of the formula (38). However, the numerical Kolmogorov length is more close to the formula $L_{KQ} \sim 2\pi q R_0 \sigma_{Chir}^{-4/3}$ given in [45].

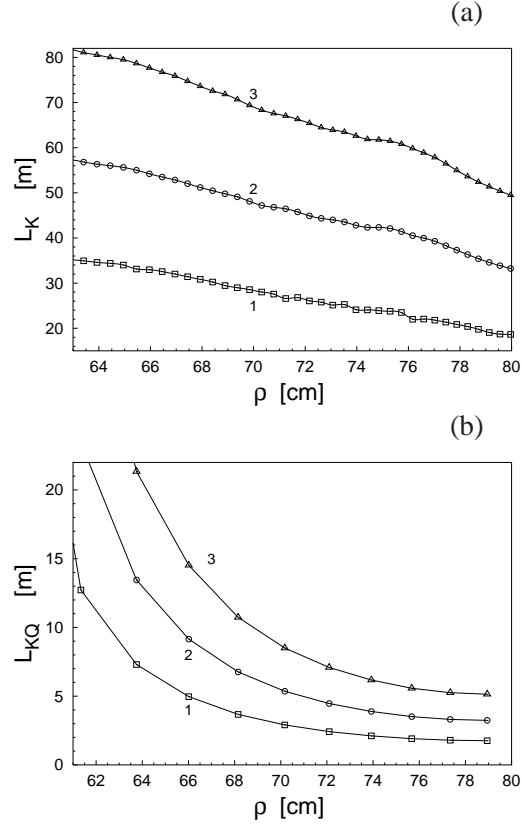


Figure 15: Radial profiles of Kolmogorov lengths, L_K , of field lines: (a) calculated numerically; (b) according to the quasilinear formula. Curves 1 to $I_d = 4.5$ kA, curves 2 and 5 – $I_d = 9$ kA, and curves 3 and 6 – $I_d = 22.5$ kA.

4 Conclusion

In summary we have studied the magnetic field structure of the ED of Tore Supra through the application of the asymptotical and mapping methods developed for the similar study of the DED of TEXTOR. To this end, an analytical model for the ergodic divertor of Tore Supra that would recover the main features of its magnetic field structure has been proposed. The fine details of the magnetic field perturbations, its poloidal and toroidal spectra in the geometrical coordinate system as well as in straight-field-line coordinates, the structure of the ergodic and laminar zone, and the field line diffusion coefficients were investigated. The use of standard code methods similar to the MASTOC code to study these detailed aspects of the magnetic field in the ED would be significantly complicated by the requirement of much higher computer power or computation times.

The decay of the magnetic field perturbations for the ED in Tore Supra was found to exhibit a power-law dependency on the radius, in contrast to an originally proposed exponential decay law. On the other hand, rigorously obtained expres-

sions for the width and the central mode of the perturbation magnetic field poloidal spectrum do coincide with the corresponding qualitatively obtained original results. An asymptotical formula describing the transformation law of the poloidal spectra was also obtained. Compared to TEXTOR-DED, where the ergodic zone at the plasma edge is formed by the interaction of only a few poloidal modes, the ED has a wide spectrum and for a given poloidal mode the radially inward decay of the perturbation was found to be much weaker.

For the Tore Supra ED, Poincaré sections, laminar plots of chaotic field lines, as well as the calculation of field line diffusion coefficients showed a highly-developed ergodic zone at the plasma edge even for relatively low perturbation currents. Similar to the case of the TEXTOR-DED, the obtained footprint plots exhibited helical stripes corresponding to the toroidal mode number and with a fractal structure. It was found that in the ergodic zone with long wall to wall connection lengths the numerical diffusion coefficients of field lines are well described by the quasilinear formula, while in the laminar zone with short wall to wall connection lengths they sharply deviate. However, for the maximum perturbation current, a different situation occurred. Already in the ergodic zone, the difference between the numerical and the quasilinear diffusion coefficient, the former exceeding the latter, monotonically increased with the radius. We have also numerically calculated the Kolmogorov lengths of field lines. They have an order of the connection lengths. However, the numerically determined Kolmogorov lengths exceeds the quasilinear prediction by factors between five and ten.

References

- [1] W. Engelhardt and W. Feneberg. Influence of an ergodic magnetic limiter on the impurity content in a tokamak. *Journal of Nuclear Materials*, 76 & 77:518–520, 1978.
- [2] W. Feneberg and G. H. Wolf. A helical magnetic limiter for boundary-layer control in large tokamaks. *Nuclear Fusion*, 21:669–676, 1981.
- [3] A. Samain, A. Grosman, and W. Feneberg. Plasma motion and purification in an ergodic divertor. *Journal of Nuclear Materials*, 111 & 112:408–412, 1982.
- [4] K. W. Gentle. The Texas experimental tokamak (TEXT) facility. *Nuclear Technology - Fusion*, 1(4):479–485, 1981.
- [5] J. S. deGrassie, N. Ohyabu, N. H. Brooks, and et al. Ergodic magnetic limiter experiments on text with a 7/3 resonance. *Journal of Nuclear Materials*, 128-129:266–270, 1984.

- [6] N. Ohyabu, J. S. DeGrassie, N. H. Brooks, and et al. Preliminary results from the ergodic magnetic limiter experiment on the TEXT experimental tokamak. *Journal Nuclear Materials*, 121:363–367, 1984.
- [7] N. Ohyabu, J. S. de Grassie, N. Brooks, and et al. Ergodic magnetic layer experiment. *Nuclear Fusion*, 25(11):1684–1688, 1985.
- [8] S. C. McCool, A. J. Wootton, A. Y. Aydemir, and et al. Electron thermal confinement studies with applied resonant fields on TEXT. *Nuclear Fusion*, 29(4):547–562, 1989.
- [9] S. C. McCool, A. J. Wootton, M. Kotschenreuther, and et al. Particle transport studies with the applied resonant fields on text. *Nuclear Fusion*, 30:167– 173, 1990.
- [10] P. Deschamps, A. Grosman, M. Lipa, and et al. Power exhaust and plasma-surface interaction control in TORE SUPRA. *Journal of Nuclear Materials*, 128-129:38–47, 1984.
- [11] A. Samain, A. Grossman, T. Blenski, G. Fuchs, and B. Steffen. An ergodic divertor for TORE-SUPRA. *Journal of Nuclear Materials*, 128 & 129:395–399, 1984.
- [12] M. Lipa, R. Aymar, P. Deschamps, et al. Mechanical design and manufacture of magnetic ergodic divertor for the Tore Supra tokamak. In A. M. Van Ingen, A. Nijssen-Vis, and H. T. Klippel, editors, *Fusion Technology. Proc. 15th Symp. Utrecht, 1988*, volume 1, pages 874–878, Amsterdam and New York, 1989. Elsevier.
- [13] A. Grosman. Heat flux exhaust in TORE SUPRA in ergodic divertor and limiter configurations. In *Fusion Energy 1998. (Proc. 17th Int. Conf. Yokohama)*, Vienna, 2000. IAEA. CD-ROM file EXP4/04 and <http://www.iaea.org/programmes/ripc/physics/start.htm>.
- [14] Ph. Ghendrih, A. Grossman, and H. Capes. Theoretical and experimental investigations of stochastic boundaries in tokamaks. *Plasma Physics and Controlled Fusion*, 38:1653 –1724, 1996.
- [15] A. Grosman. Review of experimental achievements with stochastic boundaries. *Plasma Physics and Controlled Fusion*, 41:A185–A194, 1999.
- [16] Ph. Ghendrih, M. Bécoulet, L. Costanzo, and et al. Ergodic divertor experiments on the route to steady state operation of Tore Supra. *Nuclear Fusion*, 41:1401–1412, 2001.
- [17] Ph. Ghendrih, M. Becoulet, L. Colas, , and et al. Progress in ergodic divertor operation on Tore Supra. *Nuclear Fusion*, 42:1221–1250, 2002.

- [18] T. Shoji, H. Tamai, Y. Miura, and et al. Effects of ergodization on plasma confinement in JFT-2M. *Journal of Nuclear Materials*, 196 & 198:296–300, 1992.
- [19] T. Evans, J. S. Degraessie, H. R. Garner, et al. Resonant helical divertor experiments in ohmic and auxiliary heated JIPP T-IIU plasmas. *Journal of Nuclear Materials*, 162 & 164:636–642, 1989.
- [20] S. Takamura, N. Ohnishi, H. Yamada, and T. Okuda. Electric and magnetic structure of an edge plasma in a tokamak with a helical magnetic limiter. *Physics of Fluids*, 30:144–147, 1987.
- [21] S. Takamura, Y. Shen, H. Yamada, M. Miyake, T. Tamakoshi, and T. Okuda. Electric and magnetic structure of tokamak edge plasma with static and rotating helical magnetic limiter. *Journal of Nuclear Materials*, 162-164:643–647, 1989.
- [22] Y. Shen, M. Miyake, S. Takamura, T. Kuroda, and T. Okuda. Ergodic magnetic limiter experiments in the HYBTOK-II tokamak. *Journal of Nuclear Materials*, 168:295–303, 1989.
- [23] I. L. Caldas, R. L. Viana, M. S. Araujo, and et al. Control of chaotic magnetic fields in tokamaks. *Braz. J. Phys.*, 32:980–1004, 2002.
- [24] C. J. A. Pires, E. A. O. Saettonne, M. Y. Kucinski, A. Vannucci, and R. L. Viana. Magnetic field structure in the tcabr tokamak due to ergodic limiters with a non-uniform current distribution: theoretical and experimental results. *Plasma Physics and Controlled Fusion*, 47:1609–1632, 2005.
- [25] T. Kawamura, Y. Abe, and T. Tazima. Formation of magnetic islands and ergodic magnetic layers in wall-lapping plasma as a non-divertor concept for a reactor - relevant tokamak. *Journal Nuclear Materials*, 111-112:268–273, 1982.
- [26] K. Hattori, Y. Seike, Z. Yoshida, S. Hamaguchi, H. Yamada, N. Suzuki, K. Itami, Y. Kamada, N. Inoue, and T. Uchida. Shrinkage of tokamak current channel by external ergodization. *Journal of Nuclear Materials*, 121:368–373, 1984.
- [27] K. H. Finken(ed.). Special issue: The dynamic ergodic divertor. *Fusion Engineering and Design*, 37:335–448, 1997.
- [28] K. H. Finken, S. S. Abdullaev, M. F. M. De Bock, and et al. Background and initial experiments with the Dynamic Ergodic Divertor on TEXTOR. *Fusion Science and Technology*, 47(2):87–96, 2005.
- [29] K. H. Finken, S. S. Abdullaev, M. F. M. de Bock, and et al. Overview of experiments with the Dynamic Ergodic Divertor on TEXTOR. *Contributions to Plasma Physics*, 46(7-9):515–526, 2006.

- [30] K. H. Finken, S. S. Abdullaev, W. Biel, and et al. The dynamic ergodic divertor in the TEXTOR tokamak: plasma response to dynamic helical magnetic field perturbations. *Plasma Physics and Controlled Fusion*, 46:B143–B155, 2004.
- [31] H. R. Koslowski, E. Westerhof, M. de Bock, and et al. Tearing mode physics studies applying the dynamic ergodic divertor on TEXTOR. *Plasma Physics and Controlled Fusion*, 48:B53–B62, 2006.
- [32] A. Wingen, S. S. Abdullaev, K. H., and K. H. Spatschek. Influence of stochastic fields on relativistic electrons. *Nuclear Fusion*, 46:941–952, 2006.
- [33] K. H. Finken, S. S. Abdullaev, M. Jakubowski, R. Jaspers, M. Lehnen, R. Schlikeiser, K. H. Spatschek, R. Wolf, and the TEXTOR Team. Runaway losses in ergodized plasmas. *Nuclear Fusion*, 47:91–102, 2006.
- [34] K. H. Finken, S. S. Abdullaev, M. Jakubowski, and et al. Improved confinement due to open ergodic field lines imposed by the Dynamic Ergodic Divertor in TEXTOR. *Physical Review Letters*, 98:065001, 2007.
- [35] Y. Xu, R. R. Weynants, S. Jachmich, and et al. Influence of the static Dynamic Ergodic Divertor on edge turbulence properties in TEXTOR. *Physical Review Letters*, 97:16503, 2006.
- [36] Y. Xu, M. Van Schoor, R. R. Weynants, S. Jachmich, M. Vergote, M. W. Jakubowski, P. Beyer and M. Mitri, B. Schweer, D. Reiser, B. Unterberg, K. H. Finken, M. Lehnen, and the TEXTOR team. Edge turbulence during the static dynamic ergodic divertor experiments in TEXTOR. *Nuclear Fusion*, 47(12):1696–1709, 2007.
- [37] T. E. Evans, R. A. Moyer, P. R. Thomas, and et al. Suppression of large edge-localized modes in high-confinement DIII-D plasmas with a stochastic magnetic boundary. *Physical Review Letters*, 92:235003, 2004.
- [38] T. E. Evans, R. A. Moyer, J. G. Watkins, and et al. Suppression of large edge localized modes with edge resonant magnetic fields in high confinement DIII-D plasmas. *Nuclear Fusion*, 45:595–607, 2005.
- [39] T. E. Evans, R. A. Moyer, K. H. Burrell, and et al. Edge stability and transport control with resonant magnetic perturbations in collisionless tokamak plasmas. *Nature Physics*, 2:419–423, 2006.
- [40] M. W. Jakubowski, O. Schmitz, S. S. Abdullaev, S. Brezinsek, K. H. Finken, A. Krämer-Flecken, M. Lehnen, U. Samm, K. H. Spatschek, B. Unterberg, R. C. Wolf, and the TEXTOR team. Change of the magnetic-field topology by an ergodic divertor and the effect on the plasma structure and transport. *Physical Review Letters*, 96:035004, 2006.

- [41] M. W. Jakubowski, A. Wingen, S. S. Abdullaev, K. H. Finken, M. Lehnen, K. H. Spatschek, R. C. Wolf, and the TEXTOR team. Observation of the heteroclinic tangles in the heat flux pattern of the ergodic divertor at TEXTOR. *Journal of Nuclear Materials*, 363-365:371–376, 2006.
- [42] M. W. Jakubowski, M. Lehnen, K. H. Finken, O. Schmitz, S. S. Abdullaev, B. Unterberg, R. C. Wolf, and the TEXTOR team. Influence of the dynamic ergodic divertor on the heat deposition pattern in TEXTOR at different collisionalities. *Plasma Phys. Control. Fusion*, 49:S109–S121, 2007.
- [43] A. Wingen, M. Jakubowski, K. H. Spatschek, S. S. Abdullaev, K. H. Finken, M. Lehnen, and the TEXTOR team. Traces of stable and unstable manifolds in heat flux patterns. *Physics of Plasmas*, 14:042502, 2007.
- [44] F. Nguyen, Ph. Ghendrih, and A. Samain. *Calculation of Magnetic Field Topology of Ergodized Zone in Real Tokamak Geometry. Application to the Tokamak TORE-SUPRA through the MASTOC Code*. Number DFRC/CAD Preprint EUR-CEA-FC-1539. CEA, Cadarache, 1995.
- [45] F. Nguyen, Ph. Ghendrih, and A. Grosman. Interaction of stochastic boundary layer with plasma facing components. *Nuclear Fusion*, 37:743–758, 1997.
- [46] A. Kaleck, M. Hassler, and T. Evans. Ergodization of the magnetic field at the plasma edge by the dynamic ergodic divertor. *Fusion Engineering and Design*, 37:353–378, 1997.
- [47] Th. Eich, K.H. Finken, and A. Kaleck. Modelling efforts on the helical near field divertor of the Dynamic Ergodic Divertor (DED) for TEXTOR. *Contributions to Plasma Physics*, 38:112–117, 1998.
- [48] S. S. Abdullaev, K. H. Finken, and K. H. Spatschek. Asymptotical and mapping methods in study of ergodic divertor magnetic field in a toroidal system. *Physics of Plasmas*, 6:153–174, 1999.
- [49] K. H. Finken, S. S. Abdullaev, A. Kaleck, and G. H. Wolf. Operating space of the Dynamic Ergodic Divertor for TEXTOR-94. *Nuclear Fusion*, 39:637–661, 1999.
- [50] S. S. Abdullaev, K. H. Finken, M.W. Jakubowski, et. al. Overview of magnetic structure induced by the TEXTOR-DED and the related transport. *Nuclear Fusion*, 43:299–313, 2003.
- [51] K. H. Finken, S. S. Abdullaev, M. Jakubowski, M. Lehnen, A. Nicolai, and K. H. Spatschek. *The structure of magnetic field in the TEXTOR-DED*, volume 45 of *Energy Technology*. Forschungszentrum Julich, Julich, Germany, 2005. Available online: http://www.fz-juelich.de/zb/datapool/page/439/00312_Finken.pdf.

- [52] S. S. Abdullaev. A new integration method of Hamiltonian systems by symplectic maps. *Journal of Physics A: Math. Gen.*, 32:2745–2766, 1999.
- [53] S. S. Abdullaev. The Hamilton-Jacobi method and Hamiltonian maps. *Journal of Physics A: Math. Gen.*, 35:2811–2832, 2002.
- [54] S. S. Abdullaev. *Construction of Mappings for Hamiltonian Systems and Their Applications*, volume 691 of *Lecture Notes in Physics*. Springer-Verlag, Berlin Heidelberg, 2006.
- [55] Ph. Ghendrih. Résonance du divertor ergodique. Technical Report Report EUR-CEA-FC-1537, CEA, Cadarache, 1995.
- [56] A. I. Morozov and L. S. Solov'ev. The structure of magnetic fields. In M.A. Leontovich, editor, *Reviews of Plasma Physics*, volume 2, pages 1–101, New York, 1966. Consultants Bureau.
- [57] A. H. Boozer. Evaluation of the structure of ergodic zone. *Physics of Fluids*, 26:1288–1291, 1983.
- [58] R. Balescu. *Transport processes in plasmas: 2. Neoclassical transport theory*. North-Holland, Amsterdam, 1988.
- [59] A. H. Boozer. Plasma confinement. In *Encyclopedia of Physical Science and Technology*, volume 13, New York, 1992. Academic Press.
- [60] J. Wesson. *Tokamaks*, volume 48 of *Oxford Engineering Science Series*. Clarendon Press, Oxford, 3 edition, 2004.
- [61] M. V. Fedoryuk. *Asymptotic Methods in Analysis*, volume 13 of *Encyclopaedia of Mathematical Sciences*. Springer, Berlin, 1989.
- [62] K. H. Finken and G. H. Wolf. Background, motivation, concept and scientific aims for building a dynamic ergodic divertor. *Fusion Engineering and Design*, 37:337, 1997.
- [63] B.V. Chirikov A universal instability of many-dimensional oscillator. *Physics Report*, 52:265–379, 1979.
- [64] A.J. Lichterberg and M.A. Lieberman *Regular and Stochastic Motion 2-nd Ed.*. Springer, New York, 1992
- [65] S. S. Abdullaev, Th. Eich, and K. H. Finken. Fractal structure of the magnetic field in the laminar zone of the dynamic ergodic divertor of the torus experiment for technology-oriented research (TEXTOR-94). *Physics of Plasmas*, 8:2739–2749, 2001.
- [66] R. Z. Sagdeev, D. A. Usikov, and G. M. Zaslavsky. *Nonlinear Physics. From the Pendulum to Turbulence and Chaos*, volume 5 of *Contemporary Concepts in Physics*. Harwood Academics, Chur, Switzerland, 1988.

- [67] Y. Elskens and D. F. Escande. *Microscopic Dynamics of Plasmas and Chaos*. Institute of Physics, Bristol, 2003.
- [68] S. S. Abdullaev, K. H. Finken, A. Kaleck, and K. H. Spatschek. Twist mapping for the dynamics of magnetic field lines in a tokamak ergodic divertor. *Physics of Plasmas*, 5:196–210, 1998.